Supplementary data

Du S.Y. *et al*., Roles of the different components of Mg-chelatase in abscisic acid signal transduction.

(a)

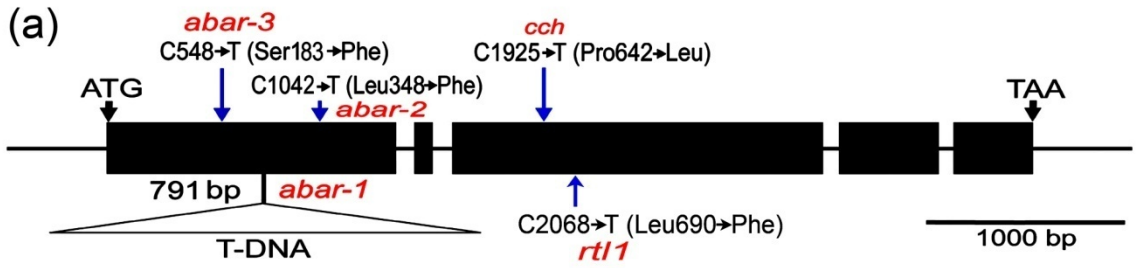

The map of the *abar* mutant alleles is shown above.

(b) **Summary of the ABA-related phenotypes of the mutant alleles**

Mutant allele	Seed germination	Early seedling growth	Stomatal movement
abar-1 (lethal)	---	--	--
abar-2	ABA insensitive	Weakly ABA insensitive	Wild-type
abar-3	ABA hypersensitive	ABA insensitive	Wild-type
cch	Weakly ABA insensitive	Weakly ABA insensitive	Strongly ABA insensitive
rtl1	Weakly ABA insensitive	Wild-type	Strongly ABA insensitive

Supplementary Fig. 1 The identified mutant alleles of *CHLH/ABAR* gene and summary of their ABA-related phenotypes. (a) Diagram showing the locations of the *abar-1*, *abar-2*, *abar-3*, *cch* and *rtl1* mutations in the CHLH/ABAR genomic DNA (modified from Wu et al., 2009). (b) Summary of the ABA-related phenotypes of these mutant alleles.

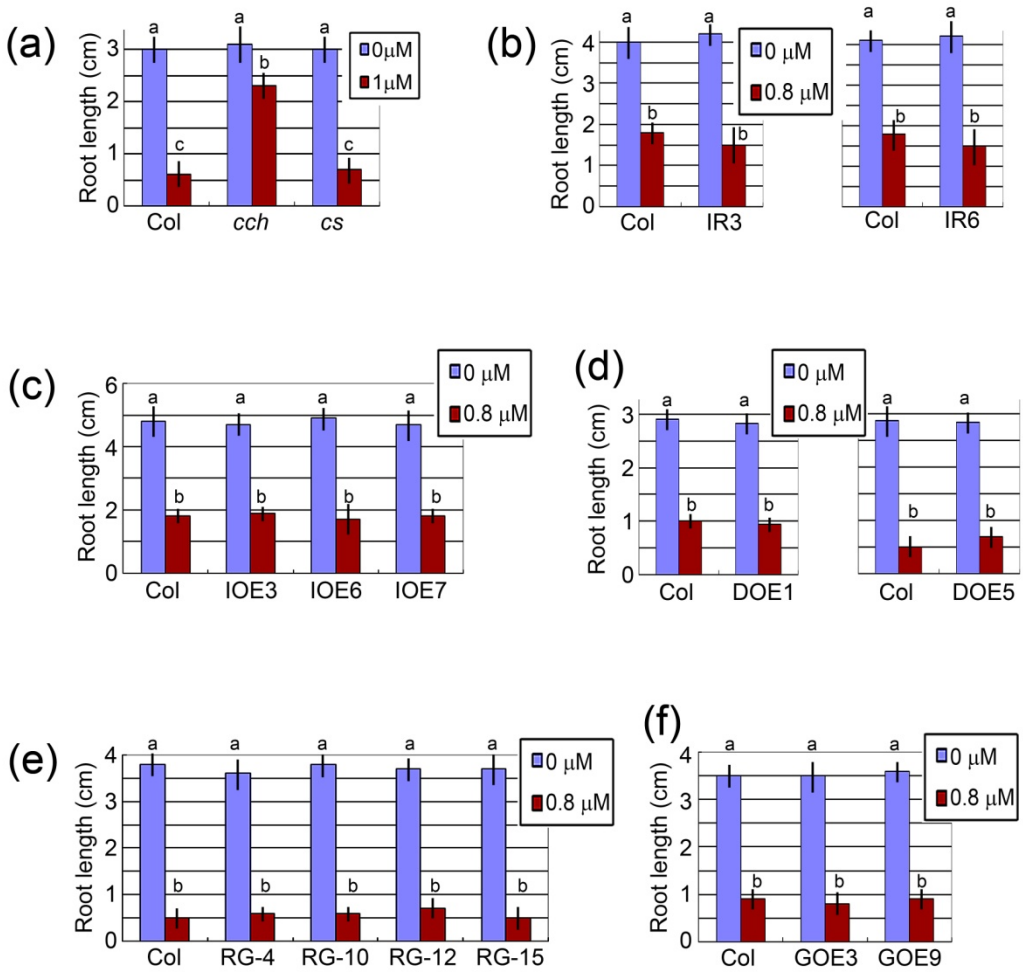

Supplementary Fig. 2 Root length of *cch*, *cs* mutants and different transgenic lines in ABA-containing medium. (a) The data for *cch* and *cs* mutants. For corresponding photos of seedling growth, see Fig. 4c. (b) The data for the *CHLI*-RNAi-transgenic lines IR3 and IR6. For corresponding photos of seedling growth, see Fig. 4d. (c) The data for the *CHLI1*-overexpression transgenic lines IOE3, IOE6 and IOE7. For corresponding photos of seedling growth, see Fig. 4e. (d) The data for the *CHLD*-overexpression transgenic lines DOE1 and DOE5. For corresponding photos of seedling growth, see Fig. 6c. (e) The data for the *GUN4*-RNAi-transgenic lines RG-4, RG-10, RG12 and RG15. For corresponding photos of seedling growth, see Fig. 7c. (f) The data for the *GUN4*-overexpression transgenic lines GOE3 and GOE9. For corresponding photos of seedling growth, see Fig. 7d.

Values are the means ± SE from three independent experiments and different letters indicate significant differences at $P < 0.05$ (Duncan's multiple range test). The experimental conditions are the same as described in the corresponding figures where the photos of the seedlings growth are presented (Fig. 4, 6, or 7).

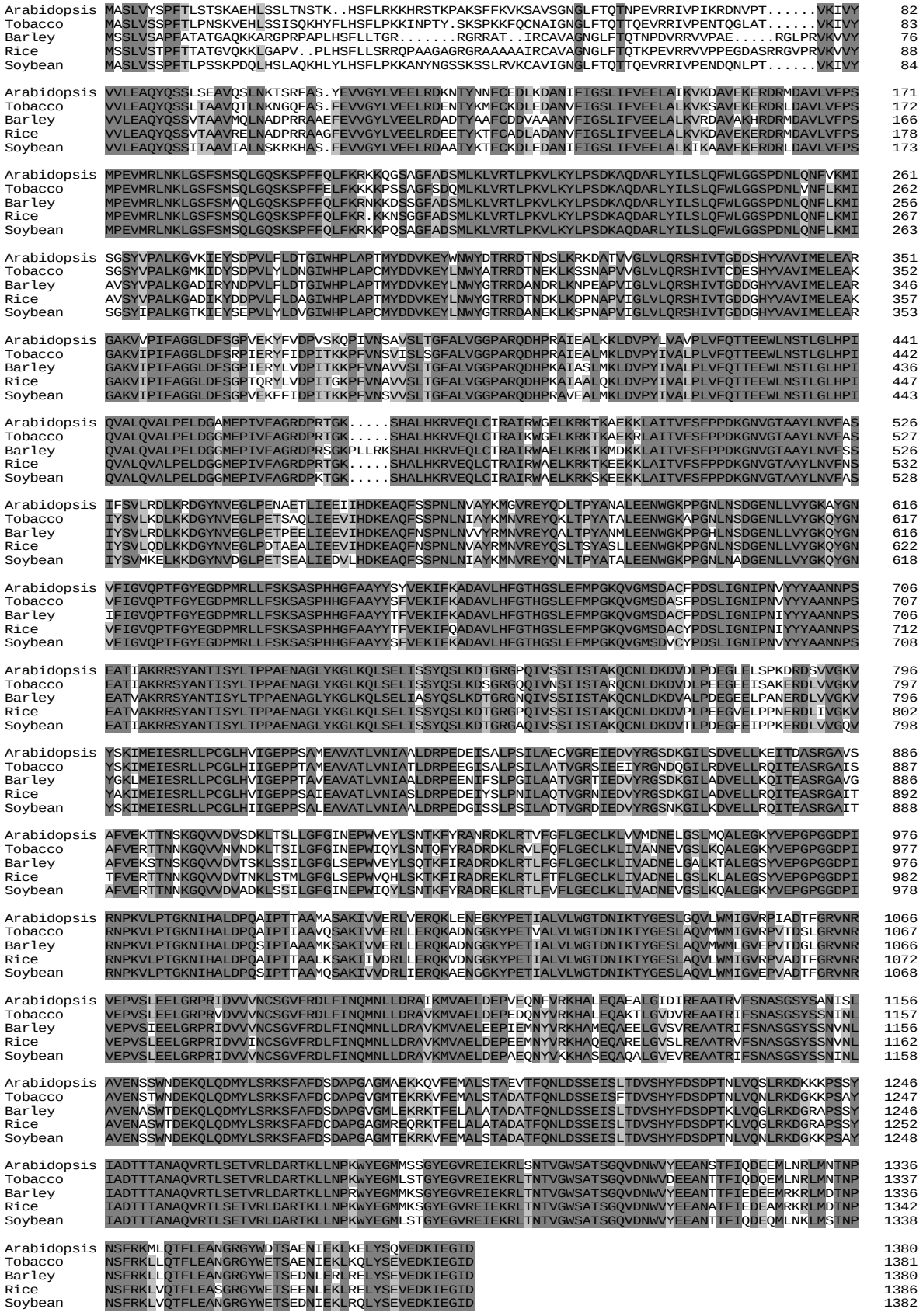

Supplementary Fig. 3 Alignment of the Amino Acid Sequence of Five Mg-Chelatase H Subunits (Identity = 89.30%).

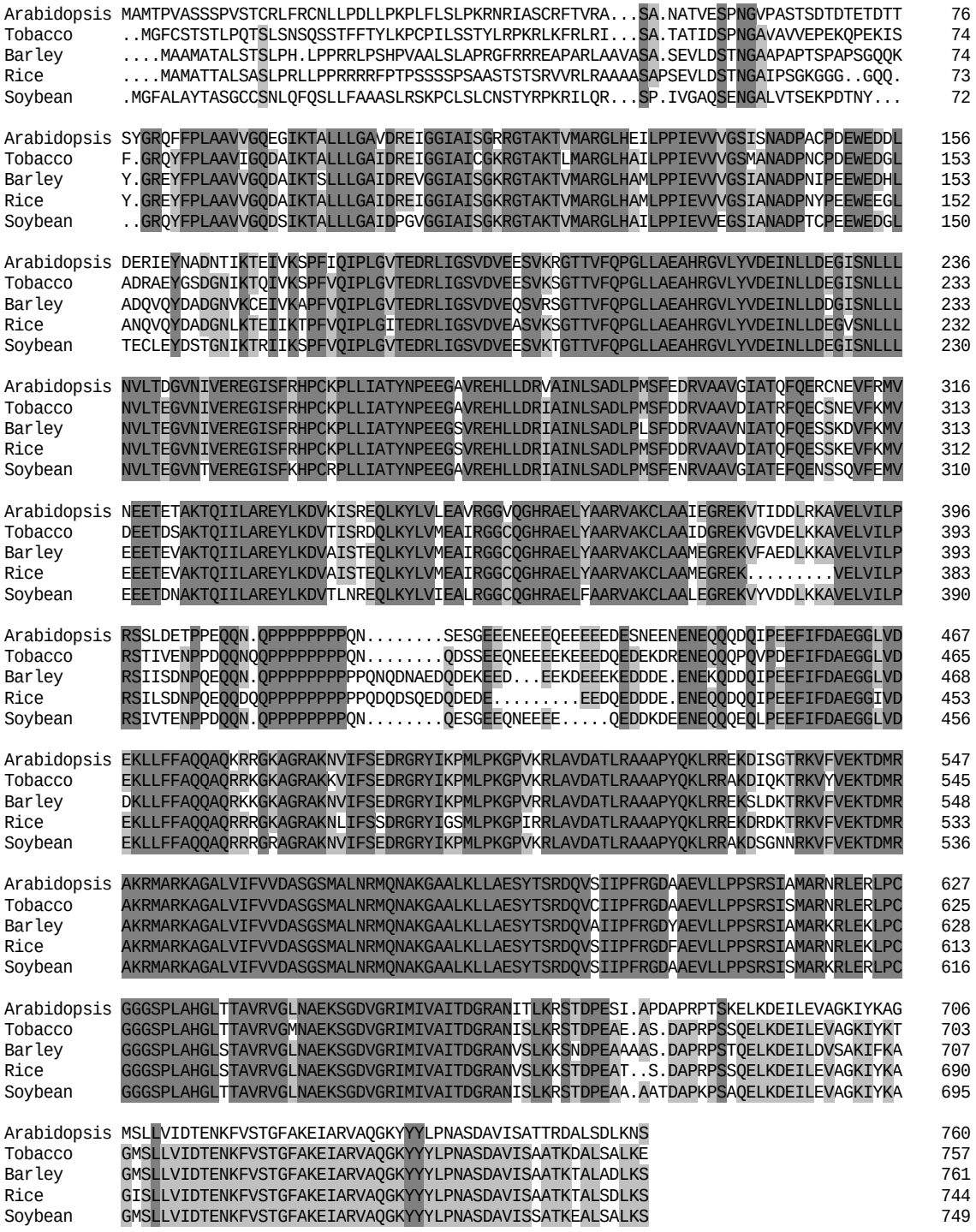

Supplementary Fig. 4 Alignment of the Amino Acid Sequence of Five Mg-Chelatase D Subunits (Identity = 82.94%).

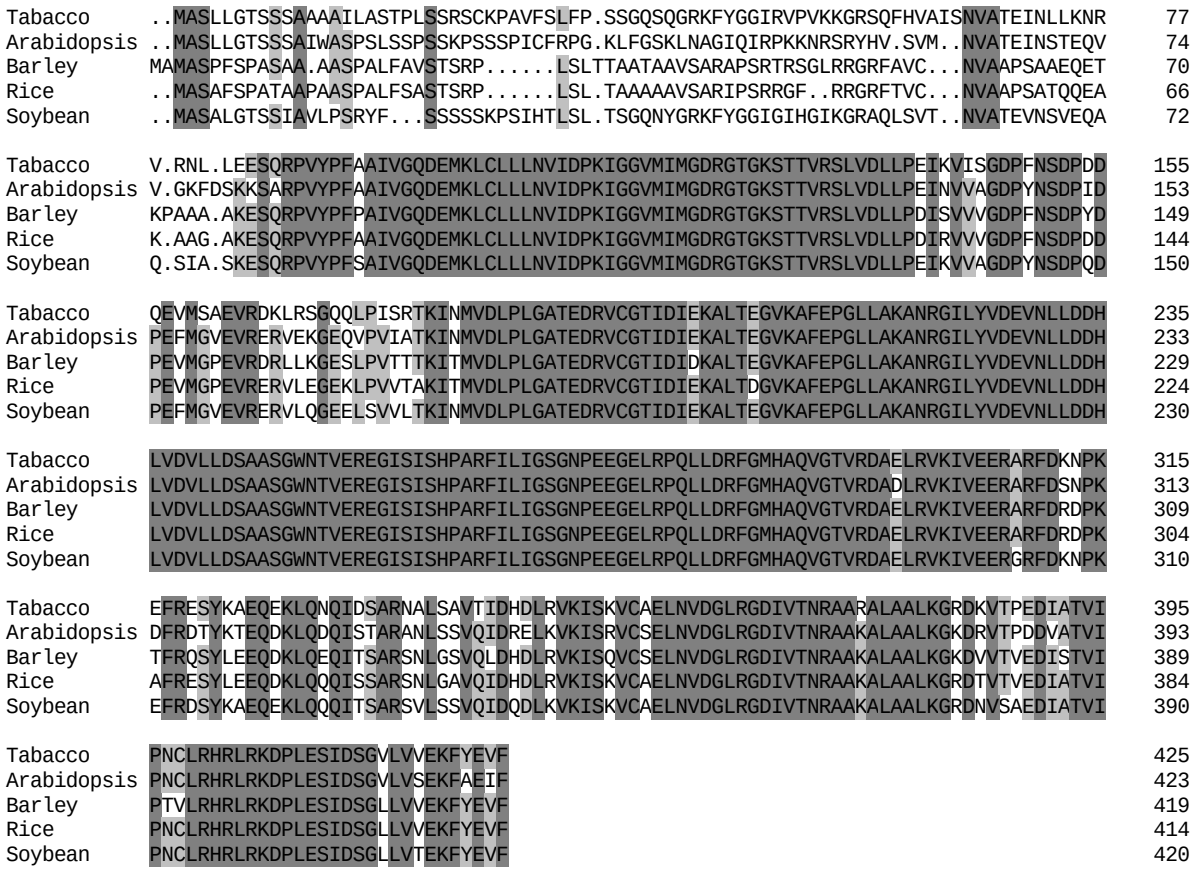

Supplementary Fig. 5 Alignment of the Amino Acid Sequence of Five Mg-Chelatase I Subunits (Identity = 82.74%).

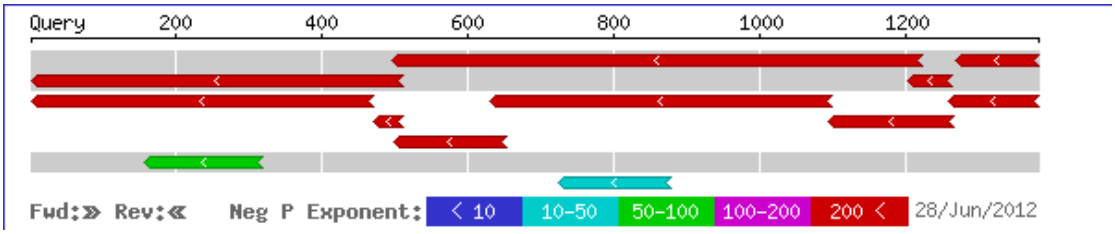

1. Alignment summary of CHLH from *Arabidopsis thaliana* and *Nicotiana benthamiana*

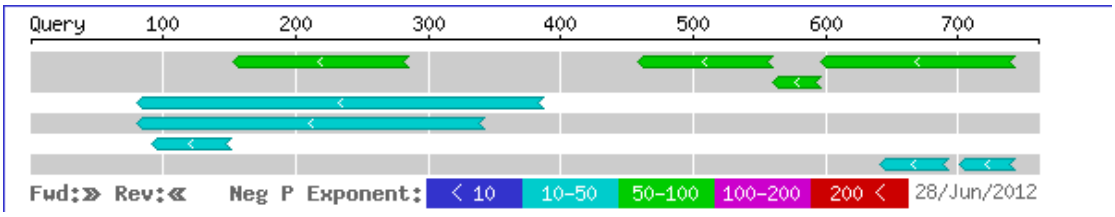

2. Alignment summary of CHLD from *Arabidopsis thaliana* and *Nicotiana benthamiana*

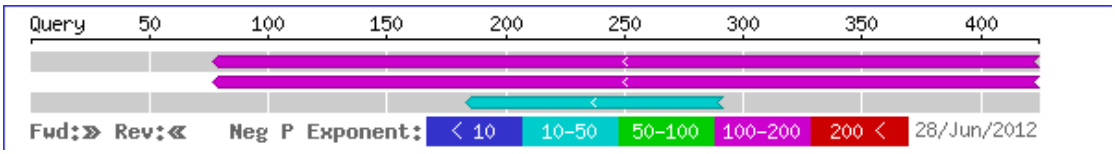

3. Alignment summary of CHLI from *Arabidopsis thaliana* and *Nicotiana benthamiana*

Supplementary Fig. 6 Alignment of the Amino Acid Sequence of Mg-Chelatase H, D and I Subunits of *Arabidopsis thaliana* and *Nicotiana benthamiana*.

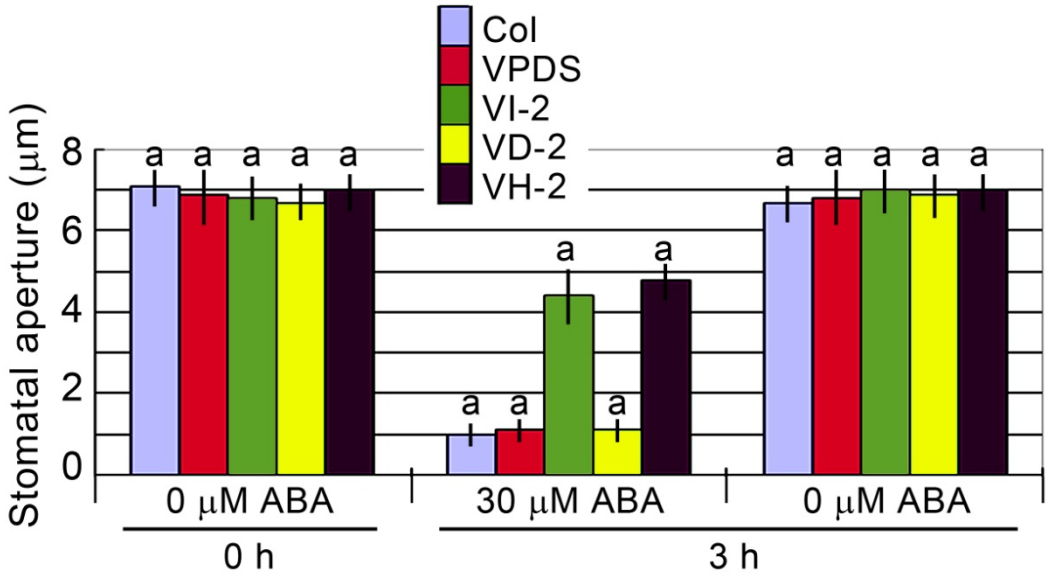

Supplementary Fig. 7 ABA-induced stomatal closure in the VIGS transgenic tobacco leaves. WT, wild-type plants; VPDS, VI-2, VD-2 and VH-2, the same transgenic lines as described in Fig. 5a. Stomatal aperture was assayed in the ABA-free medium (0 μM ABA) and ABA-containing medium (30 μM). Values are the means ± SE from three independent experiments and different letters indicate significant differences at $P < 0.05$ (Duncan's multiple range test) when comparing values within the same ABA concentration. n = 60 apertures per experiment.